Geophysical Research Letters

RESEARCH LETTER
10.1029/2018GL080716

Ocean Circulation Signatures of North Pacific Decadal Variability

Robert C. J. Wills[1], David S. Battisti[1], Cristian Proistosescu[2], LuAnne Thompson[3], Dennis L. Hartmann[1], and Kyle C. Armour[1,3]

[1]Department of Atmospheric Sciences, University of Washington, Seattle, WA, USA, [2]Joint Institute for the Study of the Atmosphere and Ocean, University of Washington, Seattle, WA, USA, [3]School of Oceanography, University of Washington, Seattle, WA, USA

Key Points:
- Decadal sea surface temperature variability in the North Pacific is linked to variability of the ocean gyre circulation
- The gyre circulation integrates white noise Aleutian Low forcing, giving variability that is strongest at decadal and longer timescales
- Sea level anomalies illustrate the ocean's role in North Pacific decadal variability

Supporting Information:
- Supporting Information S1

Correspondence to:
R. C. J. Wills,
rcwills@uw.edu

Citation:
Wills, R. C. J., Battisti, D. S., Proistosescu, C., Thompson, L., Hartmann, D. L., & Armour, K. (2019). Ocean circulation signatures of North Pacific decadal variability. *Geophysical Research Letters*, *46*, 1690–1701. https://doi.org/10.1029/2018GL080716

Received 1 OCT 2018
Accepted 7 JAN 2019
Accepted article online 15 JAN 2019
Published online 11 FEB 2019

Abstract The Pacific Decadal Oscillation (PDO) is the dominant pattern of observed sea surface temperature variability in the North Pacific. Its characteristic pattern of eastern intensified warming and cooling within the Kuroshio-Oyashio Extension is pervasive across timescales. We investigate the mechanisms for its decadal persistence in coupled climate models, focusing on the role of ocean circulation changes. We use low-frequency component analysis to isolate the mechanisms relevant at decadal and longer timescales from those acting at shorter timescales. The PDO warm phase is associated with strengthening and expansion of the North Pacific subpolar gyre in response to a deepening of the Aleutian Low. The subpolar gyre takes several years to respond to wind stress forcing through baroclinic ocean Rossby wave adjustment, such that white noise atmospheric forcing is integrated into red noise, increasing variability at long timescales. Sea level anomalies within the Kuroshio-Oyashio Extension provide an observable ocean circulation signature of North Pacific decadal variability.

Plain Language Summary North Pacific sea surface temperatures vary from decade to decade with a characteristic pattern, where temperature anomalies near North America are opposite to those off the coast of Japan. These ocean changes influence fish populations as well as climate over the surrounding land regions. Here we investigate the physical mechanisms for this sea surface temperature variability using global climate models that include interactions between the atmosphere and ocean. We find that ocean currents change together with the changes in sea surface temperature and that the time it takes for these ocean currents to adjust to changes in the prevailing wind patterns gives this variability its persistence from decade to decade.

1. Introduction

The Pacific Decadal Oscillation (PDO) index is widely used to characterize decadal shifts in climate and ecosystems within the Pacific basin and beyond. This index is computed, using empirical orthogonal functions (EOFs), as the pattern explaining the most variance in North Pacific sea surface temperatures (SSTs; Mantua et al., 1997). However, variance is maximized across all timescales, and there is an emerging body of literature suggesting that the PDO is actually the superposition of distinct physical processes operating on different timescales (Schneider & Cornuelle, 2005; Newman, 2007; Alexander et al., 2008; Newman et al., 2016). The three broad categories of processes involved are (i) air-sea heat fluxes and Ekman transport induced by atmospheric circulation anomalies, which result either from stochastic atmospheric variability or teleconnections from the tropical Pacific (Davis, 1976; Alexander, 1990; Trenberth & Hurrell, 1994; Lau & Nath, 1996; Alexander et al., 2002; Newman et al., 2016); (ii) ocean thermal inertia and the annual reemergence of temperature anomalies sequestered beneath the summer mixed layer (Namias & Born, 1970; Frankignoul & Hasselmann, 1977; Alexander & Deser, 1995); and (iii) adjustment of the upper-ocean gyre circulation in response to wind stress forcing (Latif & Barnett, 1994, 1996; Miller et al., 1998; Deser et al., 1999; Pierce et al., 2001; Schneider & Miller, 2001; Seager et al., 2001; Schneider et al., 2002; Schneider & Cornuelle, 2005; Kwon & Deser, 2007; Qiu et al., 2007; Zhang & Delworth, 2015; O'Reilly & Zanna, 2018). A better understanding of the relative contributions of these different processes at decadal timescales is needed to improve decadal climate prediction in the Pacific sector (Meehl et al., 2009, 2014; Keenlyside & Ba, 2010).

Many types of low-frequency climate variability arise from slow dynamical processes integrating higher-frequency stochastic forcing (Hasselmann, 1976). For example, Frankignoul and Hasselmann (1977) model midlatitude SST variability as a static ocean mixed-layer integrating stochastic forcing from air-sea heat fluxes. Through this mechanism, the dominant patterns of atmospheric variability imprint upon SST variability at longer timescales. Atmospheric variability, which generally has a spectrum consistent with white noise, is integrated into red noise. This "Hasselmann model" of SST variability is the continuous time equivalent of an AR(1) process. A number of studies have applied simple AR(1) models to the PDO, either representing the PDO as a single integrator responding to forcing from the El Niño–Southern Oscillation (ENSO) and/or stochastic Aleutian low forcing (e.g., Newman et al., 2003) or constructing a multivariate AR(1) model (also known as a linear inverse model) of SST anomalies throughout the Pacific (Schneider & Cornuelle, 2005; Newman, 2007; Alexander et al., 2008; Roe, 2009; Newman et al., 2016). The persistence of SST anomalies is determined to leading order by the mixed-layer heat capacity. However, ocean adjustment (i.e., process (iii) above) may lead to specific patterns of SST anomalies with persistence that is greater than that given by the local mixed-layer heat capacity.

Here, we use low-frequency component analysis (LFCA) to identify the spatial pattern of Pacific SST anomalies with the highest ratio of interdecadal "signal" to intradecadal "noise" in long control simulations of coupled climate models. This analysis is equivalent to solving for the pattern of Pacific SST variability with the greatest decadal persistence and the "reddest" power spectrum (greatest spectral slope). We find that this pattern is similar to the PDO SST anomaly pattern but that its time series has twice the decadal persistence of the PDO index. We show that the low-frequency (interdecadal) component of the PDO (LFC-PDO), isolated through this analysis, is associated with an anomaly in the North Pacific ocean gyre circulation. Finally, we construct an AR(1) model for the LFC-PDO evolution and show that it is consistent with the dynamical adjustment of the subpolar gyre to Aleutian Low wind stress forcing through the westward propagation of baroclinic ocean Rossby waves (Miller et al., 1998; Deser et al., 1999; Seager et al., 2001; Schneider et al., 2002; Qiu et al., 2007; Sasaki & Schneider, 2011).

2. Data and Methods

Low-frequency component analysis (LFCA) is a statistical method to find the linear combination of EOFs that gives the highest ratio of low-frequency to total variance (Wills et al., 2018), a specific case of signal-to-noise maximizing EOF analysis (Allen & Smith, 1997; Schneider & Griffies, 1999; Venzke et al., 1999; DelSole, 2001; Schneider & Held, 2001; Ting et al., 2009). Low-frequency variance is defined as the variance that makes it through a 10-year low-pass filter (to focus variability on decadal and longer timescales). The spatial structure of covariance in the high-frequency "noise" is used to optimally filter out high-frequency variability. The resulting anomaly patterns and time series are called low-frequency patterns (LFPs) and low-frequency components (LFCs), respectively. They are sorted by their ratio of low-frequency to total variance. The LFCs are normalized to have unit variance such that the LFPs show the anomaly pattern associated with a 1-standard-deviation anomaly in the corresponding LFC. The LFCs are required to be orthogonal (uncorrelated), but the LFPs are not. LFCA finds the pattern of variability with the maximum possible ratio of low-frequency to total variance and decadal persistence (our quantity of interest), motivating its use over other statistical methods.

We use LFCA to solve for the pattern of Pacific SST anomalies (over 45°S to 70°N) with the highest ratio of low-frequency to total variance in long preindustrial control simulations of coupled climate models from the Coupled Model Intercomparison Project phase 5 (CMIP5; Taylor et al., 2012). We include 500 years of model output from each of 26 different models (Table S1 in the supporting information) to analyze a total of 13,000 years of variability. Our methodology for applying LFCA to the CMIP5 ensemble follows that of Wills et al. (2019). To avoid issues with interpolating SST output from each model's non-Cartesian ocean grid, we use surface temperature output on each model's atmospheric grid, mask out land areas, and set all temperatures below the freezing point of sea water (indicating that sea ice is present) to the freezing point. SST anomalies are computed with respect to each model's climatological seasonal cycle such that intermodel differences in climatology and seasonal cycle are removed from the analysis. All fields are interpolated to a common (2°) analysis grid. Quadratic trends are removed from all fields before analysis to remove any influence of model drift. We include 50 EOFs of Pacific SST anomalies in the LFCA, capturing 79% of the total variance. Our results are insensitive to this choice as long as ~25 or more EOFs are included.

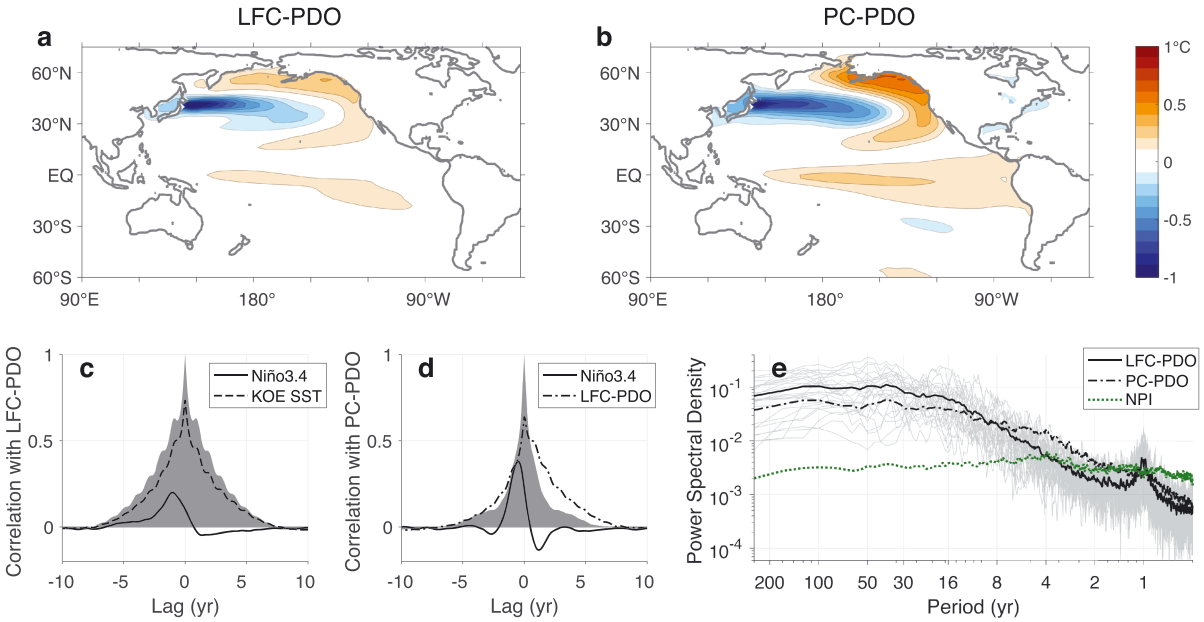

Figure 1. Low-frequency component of the PDO: (a) SST anomaly pattern associated with the leading LFC of Pacific SST anomalies (LFC-PDO) over the latitudes 45°S to 70°N, based on low-frequency component analysis with 50 EOFs retained and a 10-year low-pass cutoff. (b) SST anomaly pattern associated with the traditional (PC-PDO) definition of the PDO, based on principal component analysis of North Pacific SST anomalies over the latitudes 20–70°N. (c) and (d) Lead-lag correlations with LFC-PDO and PC-PDO, respectively. Positive lag indicates anomalies that lag the respective PDO index. Gray shading indicates the autocorrelation of each index. The KOE SST anomaly shown in (c) is averaged over 39–45°N and 140°E–180°. (e) Multimodel mean power spectra of LFC-PDO, PC-PDO, and the North Pacific Index (NPI; sea level pressure averaged over 160°E to 140°W and 30–65°N). Gray lines show the power spectra of LFC-PDO for individual models. LFC = low-frequency component; PDO = Pacific Decadal Oscillation; KOE = Kuroshio-Oyashio Extension; SST = sea surface temperature.

We estimate the significance levels of correlations and regressions by computing 500 phase randomized samples of the regressor, following Ebisuzaki (1997). Because we are using 13,000 years of monthly data, most correlations and regressions are statistically significant at the 95% confidence level.

3. The Interdecadal Component of the PDO

The leading LFC of Pacific SST anomalies (LFC-PDO) over the full Pacific domain (45°S to 70°N) in the preindustrial control ensemble shows anomalies primarily in the subpolar North Pacific (Figure 1a). Like the traditional PDO index (PC-PDO), computed as the leading principal component of North Pacific SST anomalies (20–70°N, Figure 1b), its warm (positive) phase is associated with cooling in the Kuroshio-Oyashio Extension (KOE) concurrent with warming along the west coast of North America. The KOE cooling is stronger and more geographically confined for LFC-PDO than for PC-PDO. The warming associated with LFC-PDO is about half as strong as that associated with PC-PDO but extends farther west into the Bering Sea and Sea of Okhotsk. The LFC-PDO pattern is similar to the PDO-like anomaly pattern obtained from LFCA of observed Pacific SSTs over the twentieth century (Wills et al., 2018), with the biggest difference being the larger amplitude of KOE SST anomalies in the CMIP5 models, a known bias of low-resolution climate models (Thompson & Kwon, 2010).

While the differences in spatial pattern are subtle, there are large differences in persistence between LFC-PDO and PC-PDO; LFC-PDO has greater autocorrelation at 4 years than PC-PDO has at 2 years (Figures 1c and 1d). Moreover, at lead times between 18 and 40 months, LFC-PDO is a better predictor of the PC-PDO than is the PC-PDO itself (i.e., the cross correlation exceeds the autocorrelation of PC-PDO, Figure 1d). This stems from the greater ratio of low-frequency to total variance of LFC-PDO ($r = 0.49$) compared to that of PC-PDO ($r = 0.28$); cf. $r = 0.44$ for the PDO-like LFC and $r = 0.27$ for the PC-PDO in observed Pacific SSTs (Wills et al., 2018). The longer timescale of LFC-PDO is also apparent in its power spectrum, which has approximately double the variance of PC-PDO at 16- to 100-year timescales and approximately half as much at 1.5- to 5-year timescales (Figure 1e). LFC-PDO has a redder spectrum, particularly in the vicinity of the low-pass cutoff, illustrating how LFCA isolates the reddest mode of variability. An

interesting feature within the otherwise red spectrum is the spectral peak of LFC-PDO at annual timescales, a result of the annual reemergence of SST anomalies in winter (Namias & Born, 1970; Alexander & Deser, 1995).

LFC-PDO has a squared coherence of 65% or greater with PC-PDO at all timescale longer than 10 years (Figure S1), indicating that these indices capture much of the same multidecadal variability. The greater low-frequency to total variance ratio of LFC-PDO helps to make up for the reduced amplitude of its SST anomaly pattern such that LFC-PDO explains an equal or greater fraction of low-frequency SST variance as the PC-PDO at all locations (Figure S2). In particular, the LFC-PDO explains more interdecadal SST variance than the PC-PDO throughout the western Pacific. Only in the Gulf of Alaska and along the west coast of North America does the PC-PDO explain as much interdecadal SST variance as the LFC-PDO. Furthermore, even though PC-PDO explains as much low-frequency variance in some locations, it has a lower signal-to-noise ratio and is therefore less predictable.

It has been suggested that the PDO represents the long-lived remnants of ENSO variability (Zhang et al., 1997; Vimont, 2005; Newman et al., 2016). However, Wills et al. (2018) find that the interdecadal component of the PDO in observations (identified with LFCA) is nearly independent of ENSO but is otherwise consistent with the traditional PC-PDO definition (see also Chen & Wallace, 2016). It therefore warrants investigation how strongly coupled the two PDO definitions are to ENSO in CMIP5 models. We investigate the coupling with ENSO based on lead-lag correlations of each PDO index with Niño3.4 (Figures 1c and 1d). ENSO is correlated with LFC-PDO at lead times of 0–3 years (ENSO leads) and weakly anticorrelated at lag times of 1–4 years (cf. observational analysis of Wills et al., 2018, where there is no significant correlation when ENSO leads). The peak correlation of 0.2 occurs at a lead time of 1 year (ENSO leads). The PC-PDO has a stronger peak correlation (0.4) with ENSO than LFC-PDO—at a lead time of 6 months (ENSO leads). Away from this peak correlation, the lead-lag correlation resembles the ENSO autocorrelation and therefore does not contain new information about the relationship between PC-PDO and ENSO. The exact strength of ENSO-PDO coupling depends on the indices used to define these two modes of variability, but both CMIP5 models and observations suggest that the interdecadal component of the PDO is only weakly coupled to ENSO.

Regressions of sea level pressure (SLP) and wind stress anomalies onto the LFC-PDO show that its warm phase is associated with a deepening of the Aleutian Low (Figure 2a). Characterizing the Aleutian Low by the North Pacific Index (NPI; the average SLP anomaly over the box in Figure 2a; Trenberth & Hurrell, 1994), we find that the Aleutian Low is anomalously strong for 5 years before a maximum in the LFC-PDO. The lead correlation is strongest in December–March (not shown) and decays to 0 with an e-folding time of 2–3 years. This suggests that the Aleutian Low is forcing the LFC-PDO in winter and that the LFC-PDO integrates this forcing over the prior 2–3 years. This is further supported by the coherence spectrum between NPI and LFC-PDO, which shows ~50% squared coherence on decadal and longer timescales (Figure 3a), with LFC-PDO lagging NPI by ~2 years. The decadal coherence between NPI and LFC-PDO is greater than the coherence between NPI and Niño3.4 at any timescale (Figure 3b), suggesting that the forcing of LFC-PDO by Aleutian Low internal variability is larger than the forcing by ENSO through the atmospheric bridge mechanism (Lau & Nath, 1996; Alexander et al., 2002). NPI has a white power spectrum at interannual and longer timescales, with only a small peak in the ENSO band (3–8 years, Figure 1e). Therefore, a source of persistence must exist within the North Pacific to give rise to the red power spectrum of the LFC-PDO (Hasselmann, 1976).

4. Signatures of Dynamical Ocean Adjustment in Pacific Decadal Variability

Two potential sources of SST persistence are (i) ocean thermal inertia above the maximum winter mixed-layer depth and (ii) ocean circulation dynamics. Lead-lag relationships between SST anomalies and net surface heat flux anomalies can be used to distinguish between these possibilities, as positive/negative SST anomalies must be preceded by net surface heat fluxes into/out of the ocean in the absence of a dynamic ocean circulation response. Regressions of net surface heat flux anomalies onto the LFC-PDO show the largest anomalies within the KOE, where anomalous heat fluxes into the ocean occur concurrently with negative SST anomalies (Figure 2b), including in the years leading up to and the years following a peak LFC-PDO anomaly. Cold SSTs in the KOE must be maintained by anomalous ocean heat flux divergence, because these surface heat fluxes act to warm the ocean. The anomalously warm regions to the north and east

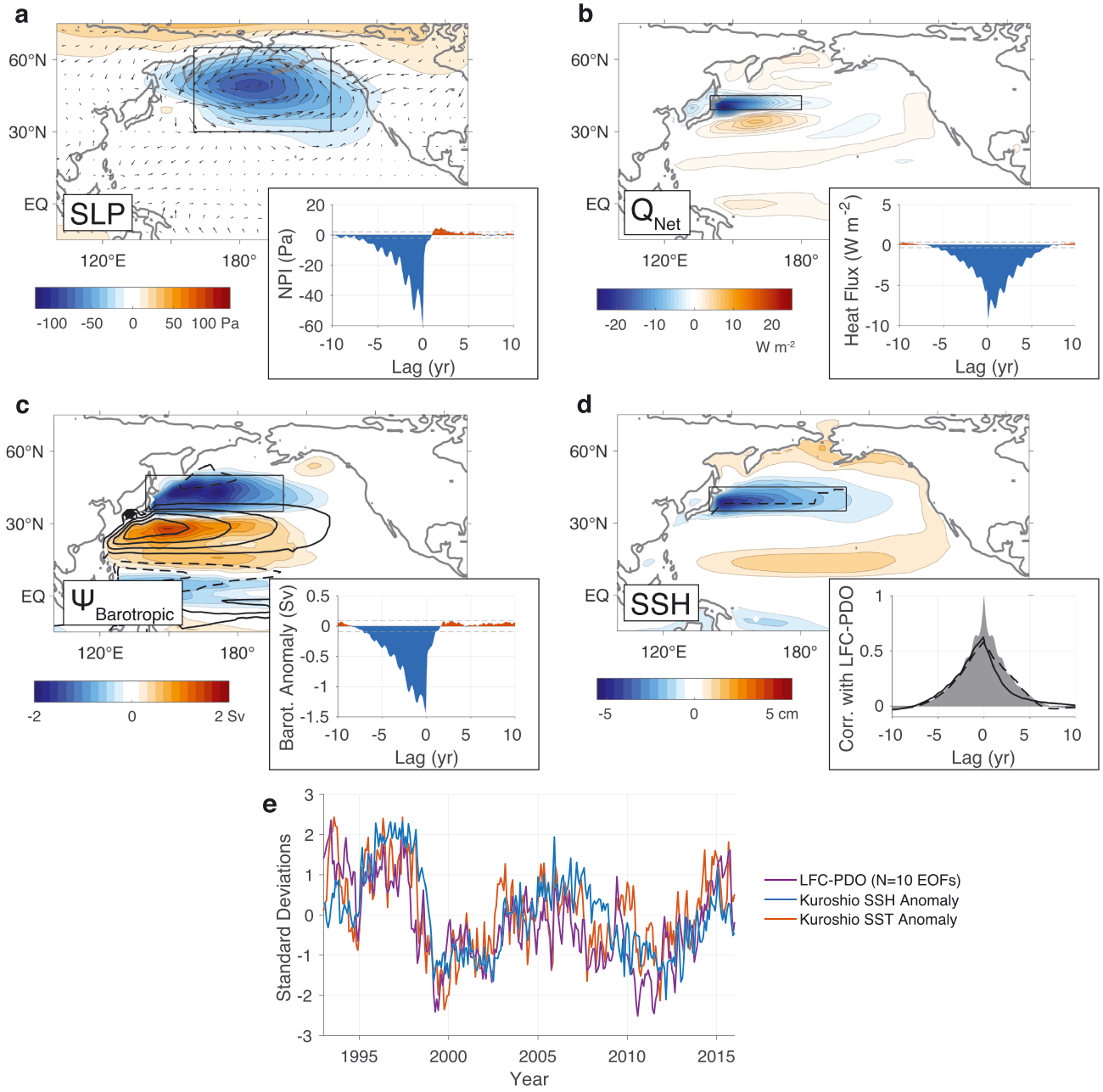

Figure 2. LFC-PDO lead-lag relationships: Lag-0 regressions of (a) SLP (shading) and wind stress (arrows), (b) net air-sea heat flux (including radiative fluxes, positive upward), (c) ocean barotropic stream function, and (d) SSH anomalies onto the LFC-PDO, showing the anomalies associated with a 1-standard-deviation LFC-PDO anomaly. The climatological ocean barotropic stream function is shown in (c) with black contours (contour interval 10 Sv, dashed negative). The latitude of maximum SSH gradient is shown in (d) with a black dashed line (for 140°E to 160°W). Insets show the lead-lag regressions of (a) the NPI, (b) the net air-sea heat flux anomaly averaged over the KOE (140°E–180°; 39–45°N), and (c) the barotropic streamfuntion anomaly averaged over the western Pacific (140°E to 160°W; 35–50°N), onto the LFC-PDO. Positive lag indicates anomalies that lag the LFC-PDO. Dashed gray horizontal lines in the insets of (a)–(c) show the 95% significance levels, computed using phase randomization (cf. Ebisuzaki, 1997). Averaging regions are shown with boxes in the corresponding map plots. The inset in (d) shows the lead-lag correlation of the LFCA-based SSH index (solid line, see also Figure S6) and the KOE SSH anomaly (dashed line, averaged over 140–160°E and 35–45°N) with LFC-PDO, compared with the LFC-PDO autocorrelation (gray shading). (e) Observed KOE SST and SSH anomalies (averaged over 140–160°E and 35–45°N, minus global mean) and an LFCA-based PDO index from Wills et al. (2018; 10 EOFs included). Kuroshio SST and SSH anomalies have their signs flipped and are normalized by their standard deviations, 0.52°C and 3.2 cm, respectively. SLP = sea level pressure; NPI = North Pacific Index; SSH = sea surface height; LFC = low-frequency component; PDO = Pacific Decadal Oscillation.

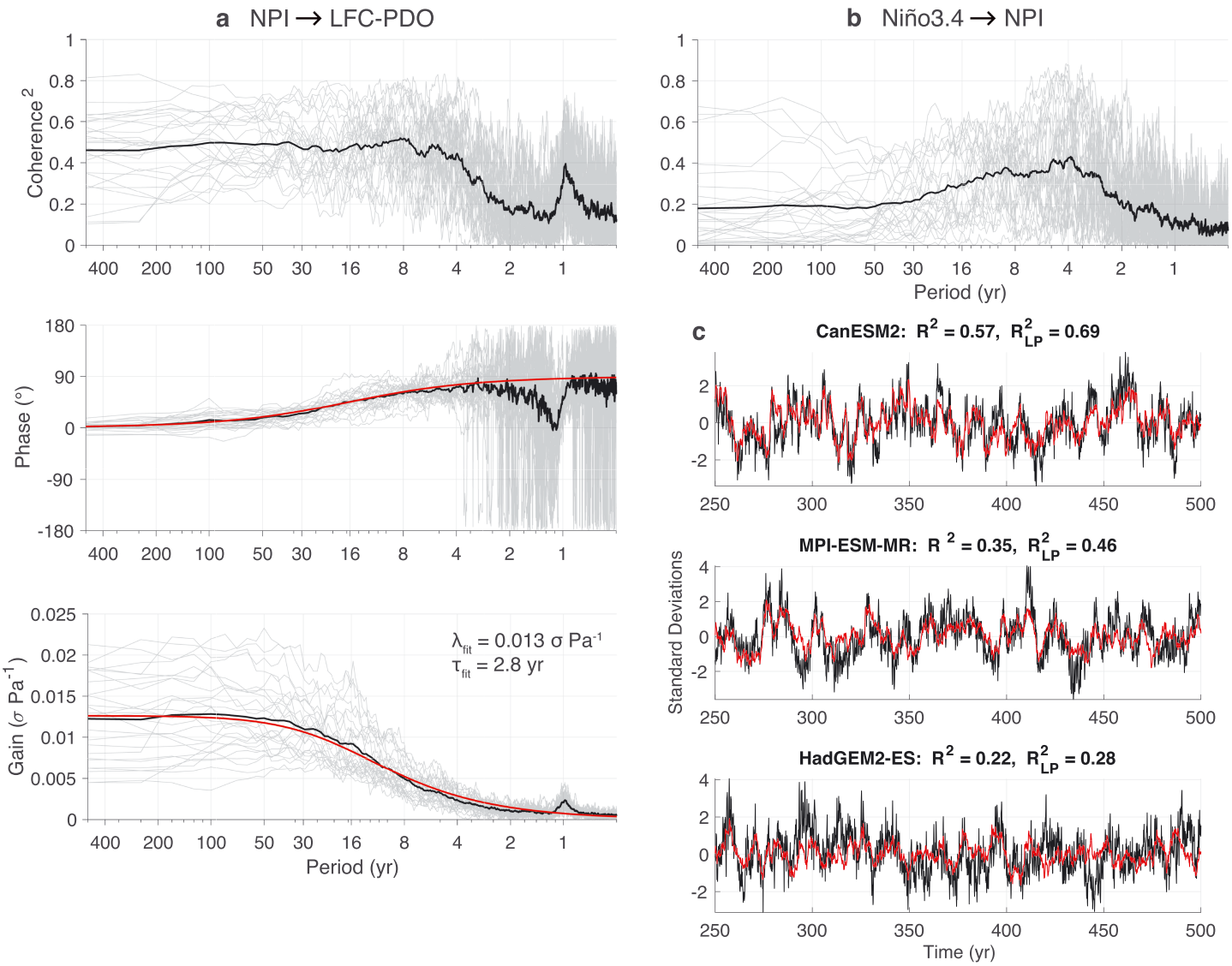

Figure 3. (a) Spectral relationships between the Aleutian Low and LFC-PDO. The Aleutian Low is characterized by the North Pacific Index (NPI; Trenberth & Hurrell, 1994). The top panel shows squared coherence. The middle panel shows phase (positive where LFC-PDO lags NPI). The bottom panel shows the frequency response function or gain (i.e., the LFC-PDO response per unit NPI anomaly). Black lines show the multimodel mean, gray lines show individual models, and red lines show the AR(1) model fit. (b) Squared coherence between NPI and El Niño (as characterized by Niño3.4). (c) Time series of LFC-PDO (black) and the NPI-forced AR(1) model fit (red) for models with good (CanESM2), average (MPI-ESM-MR), and bad (HadGEM2-ES) fits as characterized by the squared correlation (R^2) and the squared correlation after 10-year low-pass filtering (R^2_{LP}). For (c), the AR(1) model is fit in the time domain. See Figure S9 for other models. LFC = low-frequency component; PDO = Pacific Decadal Oscillation.

show small surface heat flux anomalies leading up to the maximum in the LFC-PDO and anomalous heat fluxes out of the ocean after (Figures 2b and S3). This suggests an important role for anomalous ocean heat flux convergence into these regions during the buildup and peak phases of the LFC-PDO and subsequent damping of SST anomalies by surface heat fluxes. In contrast, regression of net surface heat fluxes onto the PC-PDO shows predominantly atmospheric driven heat fluxes (i.e., heat fluxes into/out of the ocean immediately before anomalously warm/cold temperatures and out of/into the ocean immediately after), except in the KOE (Figure S4). The net surface heat flux regressions give evidence of an active role of ocean circulations in the LFC-PDO, whereas much of the PC-PDO variability can be explained by atmospheric forcing of mixed-layer temperature anomalies (Roe, 2009).

Regression of the ocean barotropic stream function onto the LFC-PDO (for the 13 models that output barotropic stream function, see Table S1) shows that the warm phase of the LFC-PDO is associated with

expansion and strengthening of the North Pacific subpolar gyre, a strengthening of the Kuroshio-Oyashio current system, and a strengthening of the North Pacific subtropical gyre (Figure 2c). The stream function anomalies are intensified on the western side of the ocean basin, consistent with a steady state Sverdrup response to wind stress forcing, where the depth-integrated geostrophic stream function is determined by the zonal integral of the wind stress curl from the eastern boundary (Sverdrup, 1947; Deser et al., 1999). The stream function anomaly has a similar time evolution to the NPI (inset in Figure 2c; cf. inset in Figure 2a) because the barotropic adjustment timescale of the ocean is fast (~2–3 months).

While the barotropic stream function gives a clear sense of ocean circulation anomalies associated with the LFC-PDO, it is difficult to observe in the real world. Sea surface height (SSH), on the other hand, is directly observed with satellite altimetry, providing insight into anomalies in the near-surface geostrophic ocean circulation and heat content. In the CMIP5 models, sea level is reduced by 5 cm per standard deviation anomaly in the LFC-PDO within the KOE, with negative anomalies of at least 1 cm extending eastward to 160°W (Figure 2d). There are weaker opposite signed anomalies in the Bering Sea, Gulf of Alaska, subtropical North Pacific, and along the west coast of North America. These SSH anomalies reflect anomalies in ocean heat content (Figure S5). The KOE SSH anomaly is strongest just to the north of the maximum climatological SSH gradient (Figure 2d), evidence of a strengthening of the Kuroshio-Oyashio current system and an expansion and strengthening of the near-surface subpolar gyre. The strengthening of the subpolar gyre circulation acts to increase heat transport into the subpolar North Pacific (Figure S3).

Sea level anomalies can be used to monitor the evolution of the gyre circulations and LFC-PDO in response to wind forcing. For the 21 models that output dynamic SSH (Table S1), we test two SSH based indices of PDO variability: (i) an index based on LFCA of Pacific SSH and (ii) the SSH anomaly within the KOE (inset in Figure 2d). The LFCA-based SSH index has a similar SSH anomaly pattern to the regression of SSH anomalies onto the LFC-PDO (Figure S6), indicating that LFCA of different variables recovers similar indices of variability. Both SSH indices are strongly correlated with the LFC-PDO and have correlations comparable to the LFC-PDO autocorrelation at lead/lag times greater than 1 year (inset in Figure 2d). SSH anomalies propagate westward, showing the baroclinic adjustment of the ocean circulation to wind stress forcing (Figure S7). In observations, the KOE SSH anomaly from satellite altimetry (Ducet et al., 2000) tracks the decadal changes in SST-based indices of the PDO from the NOAA Extended Reconstructed SST data set version 3b (Smith et al., 2008; Figure 2e), illustrating that SSH anomalies provide an observable signature of ocean circulation changes associated with the PDO.

5. Autoregressive Model of the Gyre Response to Wind Forcing

Our results suggest that the low-frequency component of the PDO comes about through the integration of Aleutian Low anomalies by baroclinic ocean circulation adjustment, a Hasselmann-type process. Here, we test whether the gain and phase relation between NPI and LFC-PDO are consistent with such a simple linear physical model. We compute the squared coherence, phase lag, and gain between NPI and the LFC-PDO based on a multitaper spectral estimator (Figure 3a). The gain shows a red noise response asymptoting to white noise at a period of ~30 years, suggesting that a Hasselmann model is appropriate.

We model the forcing of the subpolar gyre and LFC-PDO SST pattern by the Aleutian Low with a simple one-dimensional linear dynamical model of the form:

$$\tau \frac{\mathrm{dLFC}(t)}{\mathrm{d}t} = -\mathrm{LFC}(t) + \lambda \mathrm{NPI}(t) + \zeta(t). \tag{1}$$

Here LFC(t) is the LFC-PDO index, NPI(t) is the North Pacific Index of the Aleutian Low (Trenberth & Hurrell, 1994), $\zeta(t)$ is uncorrelated white noise, λ is the LFC-PDO response per unit NPI anomaly as $t \to \infty$, and τ is the LFC-PDO response timescale. This is the continuous time analog of a random walk or AR(1) process (cf. Hasselmann, 1976), which has been suggested as an appropriate model for baroclinic ocean circulation adjustment (Frankignoul et al., 1997; Qiu et al., 2007). Fluctuations in NPI(t) or $\zeta(t)$ on timescales shorter than τ are too fast to give a full response. Physically, this results when the Aleutian Low anomaly changes sign before baroclinic ocean Rossby waves have had time to communicate the anomaly to the western boundary. A key assumption of this model is that the feedback of the LFC-PDO onto NPI is small, though it could easily be generalized to include this feedback by including a second ordinary differential equation that describes the evolution of NPI(t).

By taking the Fourier transform of equation (1), we can analytically derive the transfer function $\mathcal{H}(f)$ and phase lag $\Phi(f)$ of this AR(1) model:

$$\mathcal{H}(f) = \frac{\lambda}{1 + 2\pi i \tau f} \tag{2}$$

and

$$\Phi(f) = 2\pi\tau f. \tag{3}$$

The absolute value of the transfer function gives the LFC-PDO response per unit NPI forcing in the frequency domain, that is, the gain. We obtain λ and τ through a nonlinear least squares fit of equation (2) to the computed gain, following Proistosescu et al. (2018). Each CMIP5 model is fit separately. The multimodel mean fit parameters are $\lambda = 0.013\,\sigma$ Pa^{-1} and $\tau = 2.7$ years (using σ as shorthand for standard deviations; see also the distribution of fit parameters in Figure S8). The AR(1) model provides a good fit for the gain except for the annual spectral peak (Figure 3a). It also provides a good fit for the phase lag even though it was only fit to the gain. The squared coherence (Figure 3a) gives the approximate fraction of LFC-PDO variance that is explained by this simple model (~0.5).

The timescale $\tau = 2.7$ years quantifies the response time of the LFC-PDO to Aleutian Low forcing. It is consistent with the time it takes for baroclinic ocean Rossby waves to propagate halfway across the North Pacific at the latitude of the KOE, from the region of strongest Aleutian Low forcing to the western boundary (Chelton & Schlax, 1996; Miller et al., 1998; Deser et al., 1999; Seager et al., 2001; Schneider et al., 2002; Sasaki & Schneider, 2011). The steady state response amplitude $\lambda = 0.013\,\sigma$ Pa^{-1} simply states that an ~80-Pa NPI anomaly is needed to get a 1σ LFC-PDO response, consistent with Figure 2a. We obtain similar parameters by fitting in the time domain (Figures 3c and S8). Across models, the fraction of the LFC-PDO's low-frequency variance explained by the NPI-forced AR(1) model ranges from 0.28 (in HadGEM2-ES) to 0.69 (in CanESM2), with a multimodel mean explained variance of 0.48 (Figures 3c and S9).

The PC-PDO can also be modeled with an NPI-forced AR(1) model (Figure S10), but it has a shorter response timescale $\tau = 1.1$ years (Figure S8) and therefore has a shorter timescale of predictability. Newman et al. (2003) formulate a similar model of the PDO with ENSO, rather than NPI, on the right-hand side of equation (1). This builds in an assumption that the Aleutian Low acts as a perfect intermediary between ENSO and the PDO. However, the lack of decadal coherence between Niño3.4 and NPI (Figure 3b) suggests that the atmospheric bridge is not the dominant mechanism of NPI (and thus PDO) variability on decadal timescales. We have tested a bivariate AR(1) model of the LFC-PDO, with forcing from both NPI and Niño3.4, but it shows only slight improvement over the NPI-forced AR(1) model (multimodel mean explained variance improves from 0.48 to 0.54; Figure S11).

The LFC-PDO, to a good approximation, can be understood as an integrated response to Aleutian Low forcing (i.e., an AR(1) process). Aleutian Low anomalies trigger westward propagating Rossby waves that spin-up the subpolar gyre and give characteristic SST and SSH anomaly patterns a few years later. Compared to previous studies that have studied the baroclinic adjustment of the ocean gyre circulation with simple stochastic models (e.g., Frankignoul et al., 1997; Schneider & Cornuelle, 2005; Qiu et al., 2007), the main novelty of this study is the use of LFCA to identify the pattern of Pacific SST anomalies with the greatest decadal persistence and to isolate the mechanisms of interdecadal PDO variability. We have described the interdecadal evolution of the PDO based on a single SST anomaly pattern and a univariate dynamical model (equation (1)), whereas Schneider and Cornuelle (2005) use a multivariate linear inverse model to model Pacific SST variability across timescales and Qiu et al. (2007) focus only on anomalies in the KOE.

We summarize by showing the evolution of SST and SLP anomalies throughout the warm phase of the LFC-PDO (Figure 4). The buildup phase (Years −2 to 0) is characterized by an Aleutian Low anomaly and a strengthening PDO-like SST pattern. The tropical Pacific shows maximum SST anomalies of ~0.2°C 1-year before the LFC-PDO maximum, which contribute to the Aleutian Low anomaly through the atmospheric bridge mechanism. In the years following the LFC-PDO maximum (Years 1 to 2), anomalies are limited to the high-latitude North Pacific, with a residual cooling in the KOE and warming in the Bering Sea and Gulf of Alaska. There is a positive SLP anomaly over the cold KOE region and negative SLP anomaly to the north, illustrating the atmospheric response to LFC-PDO anomalies in these low-resolution CMIP5 models. The atmospheric response is weaker, opposite signed, and smaller scale than the initial Aleutian Low forcing

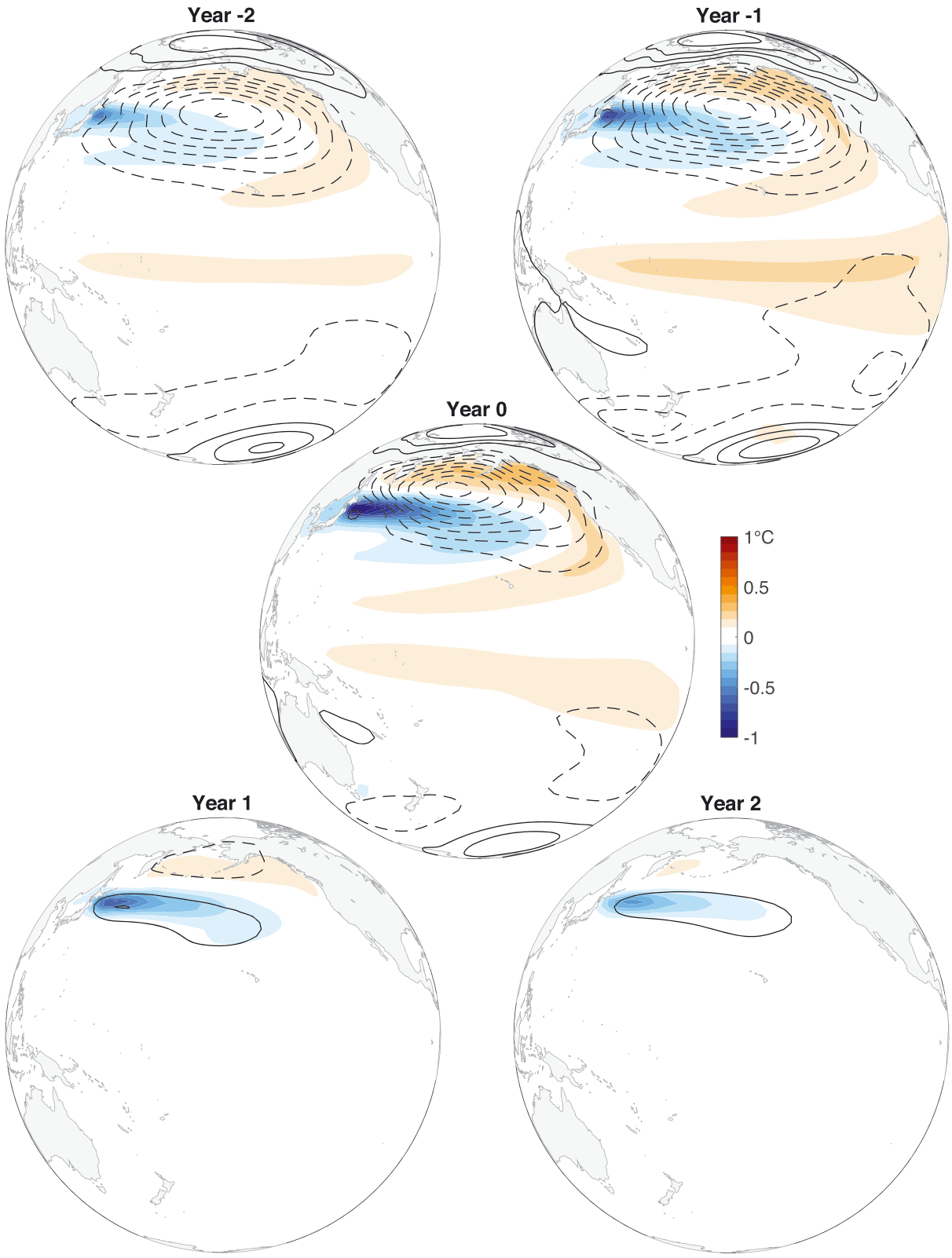

Figure 4. Evolution of the low-frequency component of the Pacific Decadal Oscillation (LFC-PDO): Regressions of sea surface temperature (shading) and sea level pressure (contours; contour interval 10 Pa; dashed negative) onto the LFC-PDO for various lead and lag times. Year 0 is the year of maximum Gulf of Alaska warming and Kuroshio-Oyashio Extension cooling as characterized by LFC-PDO.

(see also Figure 2a). Its spatial pattern is similar to observational estimates of the atmospheric response to KOE SST anomalies (e.g., Wills & Thompson, 2018), though the magnitude is weaker.

6. Discussion and Conclusions

Our results suggest that interdecadal variability of the PDO is primarily an extratropical phenomenon in CMIP5 models. The North Pacific subpolar gyre adjusts to changes in wind stress through westward ocean Rossby wave propagation, which has a characteristic timescale of 2–3 years such that KOE SSTs respond to Aleutian Low variability in an AR(1) manner. LFCA can be used to derive an index of this integrated PDO-like SST and ocean circulation response. The similarity of the LFC-PDO SST pattern with the PDO-like LFC in observations (Wills et al., 2018) suggests that these are the relevant mechanisms in the real world as well.

A key limitation of the CMIP5 models is their low resolution (∼1° ocean and ∼1–3° atmosphere), which may influence both the ocean dynamics and the atmospheric response to SST anomalies. The steady state Sverdrup balance governing the oceanic response to wind stress forcing is well resolved, though nonlinear and eddy dynamics in the KOE are not, leading to mean state biases in the KOE system and stronger and larger-scale KOE SST variability in low-resolution models than in observations and high-resolution models (Thompson & Kwon, 2010). Additionally, the low atmospheric resolution of the CMIP5 models may lead to an underestimation of the atmospheric response to KOE SST anomalies (Figure 4, Years 1–2) compared to observations (Liu et al., 2006; Frankignoul & Sennéchael, 2007; Frankignoul et al., 2011; O'Reilly & Czaja, 2015; Wills & Thompson, 2018). Several studies have shown that a higher resolution of at least ∼0.5° is needed to get the full response to sharp ocean fronts (Minobe et al., 2008; Nakamura et al., 2008; Xu et al., 2011; Smirnov et al., 2015). More work is needed to constrain the atmospheric response to KOE SST anomalies and determine if the AR(1) model of the LFC-PDO (equation (1)) remains valid for higher-resolution models and the real world. A stronger negative feedback of LFC-PDO SST anomalies onto the Aleutian Low would lead to more oscillatory behavior at decadal timescales (cf. Qiu et al., 2007).

We have found that intedecadal variability of the PDO in CMIP5 models is well explained as an integrated response to prior Aleutian Low wind stress forcing. The main way this differs from previous studies suggesting that the PDO primarily represents an integrated response of the ocean mixed layer to atmospheric heat flux forcing (Alexander et al., 2002; Newman et al., 2003; Roe, 2009) is that there is a preferred pattern of SST response to wind stress forcing set by the structure of the ocean gyres, whereas the distribution of SST anomalies in response to heat flux forcing is set by the heat fluxes themselves. While a number of previous studies have suggested that SST, SSH, and heat flux variability within the KOE represent an integrated response to prior wind stress forcing in the Aleutian Low region (e.g., Latif & Barnett, 1994; Deser et al., 1999; Seager et al., 2001; Schneider et al., 2002; Qiu et al., 2007), our work characterizes the broader structure of this variability and its relationship with the PDO. We find that SST and SSH variabilities in the KOE are highly coherent with PDO variability on decadal and longer timescales. Altimetric observations of SSH in this region provide a direct measure of the ocean circulation adjustment associated with interdecadal PDO variability. It is this ocean circulation adjustment that is responsible for the interdecadal persistence of PDO-like SST anomalies.

Acknowledgments
We thank Malte Stuecker, Dan Amrhein, and two anonymous reviewers for providing valuable feedback on this work. R. C. J. W. and D. S. B. acknowledge support from the Tamaki Foundation. R. C. J. W. and L. T. acknowledge support from NASA (Grant NNX17AH56G). R. C. J. W. and D. L. H. acknowledge support from the National Science Foundation (Grant AGS-1549579). C. P. acknowledges postdoctoral fellowship support from the University of Washington Joint Institute for the Study of the Atmosphere and Ocean. K. C. A. acknowledges support from the National Science Foundation (Grant OCE-1523641). We acknowledge the World Climate Research Programme's Working Group on Coupled Modelling, which is responsible for CMIP, and we thank the climate modeling groups (listed in Table S1 of this paper) for producing and making available their model output. The Matlab code for LFCA can be downloaded from https://github.com/rcjwills/lfca.

References

Alexander, M. A. (1990). Simulation of the response of the North Pacific Ocean to the anomalous atmospheric circulation associated with El Niño. *Climate Dynamics*, *5*(1), 53–65.

Alexander, M. A., Bladé, I., Newman, M., Lanzante, J. R., Lau, N.-C., & Scott, J. D. (2002). The atmospheric bridge: The influence of ENSO teleconnections on air-sea interaction over the global oceans. *Journal of Climate*, *15*(16), 2205–2231.

Alexander, M. A., & Deser, C. (1995). A mechanism for the recurrence of wintertime midlatitude SST anomalies. *Journal of Physical Oceanography*, *25*(1), 122–137.

Alexander, M. A., Matrosova, L., Penland, C., Scott, J. D., & Chang, P. (2008). Forecasting Pacific SSTs: Linear inverse model predictions of the PDO. *Journal of Climate*, *21*(2), 385–402.

Allen, M. R., & Smith, L. A. (1997). Optimal filtering in singular spectrum analysis. *Physics Letters A*, *234*(6), 419–428.

Chelton, D. B., & Schlax, M. G. (1996). Global observations of oceanic Rossby waves. *Science*, *272*(5259), 234–238.

Chen, X., & Wallace, J. M. (2016). Orthogonal PDO and ENSO indices. *Journal of Climate*, *29*(10), 3883–3892.

Davis, R. E. (1976). Predictability of sea surface temperature and sea level pressure anomalies over the North Pacific Ocean. *Journal of Physical Oceanography*, *6*(3), 249–266.

DelSole, T. (2001). Optimally persistent patterns in time-varying fields. *Journal of the Atmospheric Sciences*, *58*(11), 1341–1356.

Deser, C., Alexander, M. A., & Timlin, M. S. (1999). Evidence for a wind-driven intensification of the Kuroshio Current Extension from the 1970s to the 1980s. *Journal of Climate*, *12*(6), 1697–1706.
Ducet, N., Le Traon, P.-Y., & Reverdin, G. (2000). Global high-resolution mapping of ocean circulation from TOPEX/Poseidon and ERS-1 and-2. *Journal of Geophysical Research*, *105*(C8), 19,477–19,498.
Ebisuzaki, W. (1997). A method to estimate the statistical significance of a correlation when the data are serially correlated. *Journal of Climate*, *10*(9), 2147–2153.
Frankignoul, C., & Hasselmann, K. (1977). Stochastic climate models, Part II Application to sea-surface temperature anomalies and thermocline variability. *Tellus*, *29*(4), 289–305.
Frankignoul, C., Müller, P., & Zorita, E. (1997). A simple model of the decadal response of the ocean to stochastic wind forcing. *Journal of Physical Oceanography*, *27*(8), 1533–1546.
Frankignoul, C., & Sennéchael, N. (2007). Observed influence of North Pacific SST anomalies on the atmospheric circulation. *Journal of Climate*, *20*(3), 592–606.
Frankignoul, C., Sennéchael, N., Kwon, Y.-O., & Alexander, M. A. (2011). Influence of the meridional shifts of the Kuroshio and the Oyashio Extensions on the atmospheric circulation. *Journal of Climate*, *24*(3), 762–777.
Hasselmann, K. (1976). Stochastic climate models, Part I. Theory. *Tellus A*, *28*(6), 473–485.
Keenlyside, N. S., & Ba, J. (2010). Prospects for decadal climate prediction. *Wiley Interdisciplinary Reviews: Climate Change*, *1*(5), 627–635.
Kwon, Y.-O., & Deser, C. (2007). North Pacific decadal variability in the Community Climate System Model version 2. *Journal of Climate*, *20*(11), 2416–2433.
Latif, M., & Barnett, T. P. (1994). Causes of decadal climate variability over the North Pacific and North America. *Science*, *266*(5185), 634–637.
Latif, M., & Barnett, T. P. (1996). Decadal climate variability over the North Pacific and North America: Dynamics and predictability. *Journal of Climate*, *9*(10), 2407–2423.
Lau, N.-C., & Nath, M. J. (1996). The role of the "atmospheric bridge" in linking tropical Pacific ENSO events to extratropical SST anomalies. *Journal of Climate*, *9*(9), 2036–2057.
Liu, Q., Wen, N., & Liu, Z. (2006). An observational study of the impact of the North Pacific SST on the atmosphere. *Geophysical Research Letters*, *33*, L18611. https://doi.org/10.1029/2006GL026082
Mantua, N. J., Hare, S. R., Zhang, Y., Wallace, J. M., & Francis, R. C. (1997). A Pacific interdecadal climate oscillation with impacts on salmon production. *Bulletin of the American Meteorological Society*, *78*(6), 1069–1079.
Meehl, G. A., Goddard, L., Boer, G., Burgman, R., Branstator, G., Cassou, C., et al. (2014). Decadal climate prediction: An update from the trenches. *Bulletin of the American Meteorological Society*, *95*(2), 243–267.
Meehl, G. A., Goddard, L., Murphy, J., Stouffer, R. J., Boer, G., Danabasoglu, G., et al. (2009). Decadal prediction: Can it be skillful? *Bulletin of the American Meteorological Society*, *90*, 1467–1485.
Miller, A. J., Cayan, D. R., & White, W. B. (1998). A westward-intensified decadal change in the North Pacific thermocline and gyre-scale circulation. *Journal of Climate*, *11*(12), 3112–3127.
Minobe, S., Kuwano-Yoshida, A., Komori, N., Xie, S.-P., & Small, R. J. (2008). Influence of the Gulf Stream on the troposphere. *Nature*, *452*(7184), 206–209.
Nakamura, H., Sampe, T., Goto, A., Ohfuchi, W., & Xie, S.-P. (2008). On the importance of midlatitude oceanic frontal zones for the mean state and dominant variability in the tropospheric circulation. *Geophysical Research Letters*, *35*, L15709. https://doi.org/10.1029/2008GL034010
Namias, J., & Born, R. M. (1970). Temporal coherence in North Pacific sea-surface temperature patterns. *Journal of Geophysical Research*, *75*(30), 5952–5955.
Newman, M. (2007). Interannual to decadal predictability of tropical and North Pacific sea surface temperatures. *Journal of Climate*, *20*(11), 2333–2356.
Newman, M., Alexander, M. A., Ault, T. R., Cobb, K. M., Deser, C., Di Lorenzo, E., et al. (2016). The Pacific Decadal Oscillation, revisited. *Journal of Climate*, *29*(12), 4399–4427.
Newman, M., Compo, G. P., & Alexander, M. A. (2003). ENSO-forced variability of the Pacific decadal oscillation. *Journal of Climate*, *16*(23), 3853–3857.
O'Reilly, C. H., & Czaja, A. (2015). The response of the Pacific storm track and atmospheric circulation to Kuroshio Extension variability. *Quarterly Journal of the Royal Meteorological Society*, *141*(686), 52–66.
O'Reilly, C. H., & Zanna, L. (2018). The signature of oceanic processes in decadal extratropical SST anomalies. *Geophysical Research Letters*, *45*, 7719–7730. https://doi.org/10.1029/2018GL079077
Pierce, D., Barnett, T., Schneider, N., Saravanan, R., Dommenget, D., & Latif, M. (2001). The role of ocean dynamics in producing decadal climate variability in the North Pacific. *Climate Dynamics*, *18*(1-2), 51–70.
Proistosescu, C., Donohoe, A., Armour, K. C., Roe, G. H., Stuecker, M. F., & Bitz, C. M. (2018). Radiative feedbacks from stochastic variability in surface temperature and radiative imbalance. *Geophysical Research Letters*, *45*, 5082–5094. https://doi.org/10.1029/2018GL077678
Qiu, B., Schneider, N., & Chen, S. (2007). Coupled decadal variability in the North Pacific: An observationally constrained idealized model. *Journal of Climate*, *20*(14), 3602–3620.
Roe, G. (2009). Feedbacks, timescales, and seeing red. *Annual Review of Earth and Planetary Sciences*, *37*, 93–115.
Sasaki, Y. N., & Schneider, N. (2011). Decadal shifts of the Kuroshio Extension jet: Application of thin-jet theory. *Journal of Physical Oceanography*, *41*(5), 979–993.
Schneider, N., & Cornuelle, B. D. (2005). The forcing of the Pacific decadal oscillation. *Journal of Climate*, *18*(21), 4355–4373.
Schneider, T., & Griffies, S. M. (1999). A conceptual framework for predictability studies. *Journal of Climate*, *12*(10), 3133–3155.
Schneider, T., & Held, I. M. (2001). Discriminants of twentieth-century changes in Earth surface temperatures. *Journal of Climate*, *14*(3), 249–254.
Schneider, N., & Miller, A. J. (2001). Predicting western North Pacific ocean climate. *Journal of Climate*, *14*(20), 3997–4002.
Schneider, N., Miller, A. J., & Pierce, D. W. (2002). Anatomy of North Pacific decadal variability. *Journal of Climate*, *15*(6), 586–605.
Seager, R., Kushnir, Y., Naik, N. H., Cane, M. A., & Miller, J. (2001). Wind-driven shifts in the latitude of the Kuroshio-Oyashio extension and generation of SST anomalies on decadal timescales. *Journal of Climate*, *14*(22), 4249–4265.
Smirnov, D., Newman, M., Alexander, M. A., Kwon, Y.-O., & Frankignoul, C. (2015). Investigating the local atmospheric response to a realistic shift in the Oyashio sea surface temperature front. *Journal of Climate*, *28*(3), 1126–1147.
Smith, T. M., Reynolds, R. W., Peterson, T. C., & Lawrimore, J. (2008). Improvements to NOAA's historical merged land–ocean surface temperature analysis (1880–2006). *Journal of Climate*, *21*(10), 2283–2296.

Sverdrup, H. U. (1947). Wind-driven currents in a baroclinic ocean; with application to the equatorial currents of the eastern Pacific. *Proceedings of the National Academy of Sciences of the United States of America*, *33*(11), 318–326.

Taylor, K. E., Stouffer, R. J., & Meehl, G. A. (2012). An overview of CMIP5 and the experiment design. *Bulletin of the American Meteorological Society*, *93*(4), 485–498.

Thompson, L. A., & Kwon, Y.-O. (2010). An enhancement of low-frequency variability in the Kuroshio–Oyashio Extension in CCSM3 owing to ocean model biases. *Journal of Climate*, *23*(23), 6221–6233.

Ting, M., Kushnir, Y., Seager, R., & Li, C. (2009). Forced and internal twentieth-century SST trends in the North Atlantic. *Journal of Climate*, *22*(6), 1469–1481.

Trenberth, K. E., & Hurrell, J. W. (1994). Decadal atmosphere-ocean variations in the Pacific. *Climate Dynamics*, *9*(6), 303–319.

Venzke, S., Allen, M. R., Sutton, R. T., & Rowell, D. P. (1999). The atmospheric response over the North Atlantic to decadal changes in sea surface temperature. *Journal of Climate*, *12*(8), 2562–2584.

Vimont, D. J. (2005). The contribution of the interannual ENSO cycle to the spatial pattern of decadal ENSO-like variability. *Journal of Climate*, *18*(12), 2080–2092.

Wills, R. C. J., Armour, K. C., Battisti, D. S., & Hartmann, D. L. (2019). Ocean-atmosphere dynamic coupling fundamental to the Atlantic Multidecadal Oscillation. *Journal of Climate*, *32*(1), 251–272.

Wills, R. C., Schneider, T., Wallace, J. M., Battisti, D. S., & Hartmann, D. L. (2018). Disentangling global warming, multidecadal variability, and El Niño in Pacific temperatures. *Geophysical Research Letters*, *45*, 2487–2496. https://doi.org/10.1002/2017GL076327

Wills, S. M., & Thompson, D. W. (2018). On the observed relationships between wintertime variability in Kuroshio–Oyashio Extension sea surface temperatures and the atmospheric circulation over the North Pacific. *Journal of Climate*, *31*(12), 4669–4681.

Xu, H., Xu, M., Xie, S.-P., & Wang, Y. (2011). Deep atmospheric response to the spring Kuroshio over the East China Sea. *Journal of Climate*, *24*(18), 4959–4972.

Zhang, L., & Delworth, T. L. (2015). Analysis of the characteristics and mechanisms of the Pacific Decadal Oscillation in a suite of coupled models from the Geophysical Fluid Dynamics Laboratory. *Journal of Climate*, *28*(19), 7678–7701.

Zhang, Y., Wallace, J. M., & Battisti, D. S. (1997). ENSO-like interdecadal variability: 1900–93. *Journal of Climate*, *10*(5), 1004–1020.